PAPER • OPEN ACCESS

Acoustic emission source localisation for structural health monitoring of rail sections based on a deep learning approach

To cite this article: Harsh Mahajan and Sauvik Banerjee 2023 *Meas. Sci. Technol.* **34** 044010

View the article online for updates and enhancements.

Acoustic emission source localisation for structural health monitoring of rail sections based on a deep learning approach

Harsh Mahajan*⊙ and Sauvik Banerjee

Department of Civil Engineering, Indian Institute of Technology Bombay, Mumbai 400076, India

E-mail: mahajanharsh1909@gmail.com

CrossMark

Abstract

An acoustic emission (AE) approach for non-destructive evaluation of structures has been developed over the last two decades. In complex structures, one of the limitations of AE testing is to find the location of the AE source. Time of flight and wave velocity are typically employed to localise AE sources. However, complex rail structures generate multiple wave modes travelling at varying speeds, making localisation difficult. In this paper, the challenge of localisation has been split into two parts: (a) identification of the AE source zone, i.e. head, web or foot, and (b) identification of location along the length of the rail. AE events are simulated using a pencil lead break (PLB) as the source. Three models including an artificial neural network and 1D and 2D convolutional neural networks (CNNs) are trained and tested using AE signals generated by PLB sources. The accuracy of zone identification is reported as 94.79% when using the 2DCNN algorithm. For location classification it is also found that 2DCNN performed best with 73.12%, 79.37% and 67.50% accuracy of localising the AE source along the length in the head, web and foot, respectively. For AE signal generation from actual damage in a rail, a bending test on an inverted damaged rail section was then performed with loads of 100 kN, 150 kN and 200 kN. For all loads, the 2DCNN model resulted in accurate prediction of the zone of the AE source, and it accurately predicted the AE source location along the length for the loads of higher intensity (150 kN, 200 kN). It is envisaged that the deep learning approach presented in this research work will be helpful in developing a real-time monitoring system for rail inspection based on AE.

Keywords: non-destructive testing, acoustic emission, rail health monitoring, damage localisation, deep learning application, data-driven solution

(Some figures may appear in colour only in the online journal)

---

* Author to whom any correspondence should be addressed.

1. Introduction

A railroad network is a cost-effective, time-efficient and dependable form of transportation. It connects major cities, ports, industrial centres and distant locations, thereby boosting a country's economy tremendously. Rail transportation safety must be addressed to minimise the direct and indirect expenses associated with rail failure. Safety can be achieved by monitoring and maintaining rails on a regular basis. Traditionally, the ultrasonic method is used to detect the presence of a fault in a rail section based on backscattering from damage. However, the cascading effect of a surface crack over major damage, low efficiency and the slow speed of testing limit the effective use of the current technique. Acoustic emission (AE) is a rapidly advancing, non-destructive testing method used to monitor structures in service. AE is a transient wave which is produced when stored energy is suddenly released from damage under service loads. The AE waves propagate through the rail and carry information regarding the damage through various wave properties. Analysing the wave parameters of AE signals and correlating them with damage parameters can help to understand the damage mechanism and characteristics.

Over the last two decades, substantial research has been carried out to monitor rail cracks using AE technology. Initially, Bruzelius and Mba [1] explored the possibility of the application of AE technology through a small test rig. This study provided the rationale for using AE signals for rail testing. Bollas *et al* [2] presented raw data from sensors mounted on wheels and concluded that the bigger the size of the defect, the larger the number of AE hits. Zhang *et al* [3] investigated the effect of distance, depth and type of simulated AE source in rails. The complications of noise in AE signals and a wavelet-based denoising technique have been studied by Hao *et al* [4]. Using the wavelet transform method, Bianchi *et al* [5] investigated the extraction of an AE signal generated due to rolling contact fatigue. Kuang *et al* [6] investigated an AE-based crack monitoring strategy utilising wavelet entropy. Li *et al* [7] demonstrated a method for crack size determination in rail steel using wavelet packet analysis of AE signals generated during crack opening and closing in a steel bar sample. Zhang *et al* [8] proposed a long short-term memory network-based method to eliminate noise interference from AE signals and demonstrated its effectiveness in actual application. Zhang and colleagues also proposed [9] a parameter-optimised variational mode decomposition method to decompose AE signals.

In general, damage in any structure can be characterised by its type, location and severity. Locating damage is a vital part of the qualitative and quantitative analysis of damage. In the case of AE, location becomes more crucial for filtering out signals from a relevant source. A few researchers have looked at the localisation problem in AE testing. Using the least squares method, Ohtsu and Ono [10] developed a technique to determine the location of an AE source due to a tensile crack. The technique was based on the amplitude of P-waves. Using a local Newton iterative method, Ciampa and Meo [11] utilised

the time of arrival of the flexural A_o mode in a composite plate to identify the location of the AE source. Dehghan Niri and Salamone [12] proposed a probabilistic framework by considering the time of flight and wave velocity as Gaussian random variables. They used continuous wavelet transform (CWT) and an extended Kalman filter to iteratively estimate the AE source location. Mostafapour *et al* [13] used the cross time–frequency spectrum and calculated the time delay between signals and the corresponding frequency to obtain wave velocity at a specified frequency. To locate AE sources in composite structures, Al-Jumaili *et al* [14] presented a fully automatic delta T mapping technique using clustering algorithms. Mirgal *et al* [15] used a planar source localisation algorithm and particle swarm optimisation techniques to locate AE sources in concrete structures.

Currently, most localisation techniques are based on wave velocity and time of flight. These are limited to planar structures. For complex structures such as rails, it is very difficult to analyse and determine the location of the AE source for various reasons, such as the complex geometry of the rail, the wide frequency band of AE signals and numerous sources of AE signals and noise. A rail serves as a complex waveguide resulting in high dispersion, especially because of the presence of numerous modes travelling at close wave velocities for a given frequency. An AE wave is a combination of various frequencies, which in turn makes localisation a very complicated task. The AE approach can be incorporated into the real-time condition monitoring of a rail section by using the appropriate tools. AE testing generates an enormous number of data which are complex to analyse in a conventional manner. However, large datasets also provide leverage to utilise machine learning (ML) and deep learning algorithms, which are subsets of artificial intelligence (AI)-based techniques. AI can be helpful in mapping various parameters of AE waves to the damage parameters such as location, severity and so forth. The application of ML and deep learning algorithms to solve complex problems in the domain of structural health monitoring and fault detection has been growing in recent years [16–22]. Ebrahimkhanlou *et al* [23] utilised deep stacked encoders to determine coordinates of AE sources in an aluminium plate observing 100% accuracy for zonal localisation. Yang and Xu developed a stacked denoising autoencoder-based approach for AE source localisation in metallic plates with a laser cladding layer. Hesser *et al* [24] demonstrated the application of deep neural networks for source identification and zonal localisation in plate structures. Sikdar *et al* [25] proposed a convolutional neural network (CNN)-based algorithm for identification of the region of damage in a composite panel. Barbosh *et al* [26] utilised a combination of the CWT and a deep neural network to detect the location of damage in wooden beams, wooden plates and concrete beams. The application of ML in the monitoring of rails is rather sparse. Recently, Li *et al* [27] developed a multi-branch CNN to automatically classify AE waves in rails generated due to impact, crack propagation and operational noise. Using ultrasonic guided waves generated through surface-bonded piezoelectric sensors, Mahajan

and Banerjee [28] applied ML algorithms to detect damage parameters in rails. Localisation approaches based on the time of flight and velocity of wave modes are typically limited to simple geometries with well-defined dispersion characteristics, such as bars, plates and cylinders. High dispersion, i.e. the occurrence of several wave modes at a specific frequency, prevents implementation of a velocity-based approach for localising AE sources in rails. The recent literature demonstrates that the use of deep learning in such a complex problem is increasing due to its capability to capture pattern change in the input with respect to various external conditions. This research proposes employing a deep learning algorithm trained by an artificial AE source to solve the localisation problem. The capability of the algorithm is then evaluated by locating the source of the AE signal created by actual crack opening in a rail section under a load.

The overall localisation problem has been divided into two parts: first, the AE source zone is identified then the source is located along the length of the rail. Three models are proposed for zone identification and localisation of the AE source along the length based on the combination of signal features and AI techniques, including an artificial neural network (ANN), a 1D convolutional neural network (1DCNN) and a 2D convolutional neural network (2DCNN). For the simulated AE source, a pencil-lead break (PLB) is chosen for the study. PLB sources are reliable for the calibration of sensors and help in understanding AE wave propagation in any structure [29]. AE signals generated by a PLB source are recorded and denoised using an elliptical filter. Afterwards, deep learning algorithm-based classification strategies are employed to identify the AE source zone in a rail using PLB signals. After training and testing various models, the most accurate algorithm is deployed to estimate the zone and location of the AE source generated in a rail due to crack opening under a bending load. This paper is organised as follows. The experimental setups are discussed in section 2. The proposed methodologies are presented and discussed in section 3. An overview of signal processing and data preparation is presented in section 4. The results and discussion are presented in section 5, followed by the conclusion and scope of future work in section 6.

2. Experimental setup

2.1. Experimental setup for an artificial AE source

A pencil lead of diameter 0.5 mm and length 3 mm was used for the PLB experiment. The lead was pressed against a surface at 45°, breaking it due to the reaction of the collet of a mechanical pencil. WSα sensors manufactured by Physical Acoustics were used with a characteristic operating frequency between 100 and 1000 kHz and an operational temperature in the range $-65\,^\circ$C to $+177\,^\circ$C. This range of temperature ensures the workability of sensors in field testing. The AE signal generated due to the PLB was acquired through two sensors placed at 50 mm and 100 mm from the centre of the provided damage in the rail. The web was chosen for mounting

the sensors as it was more accessible and less affected by train vibration, lateral forces and high temperature compared with the head. The sensors were then connected to the PAC AE system through a pre-amplifier with gain of 40 dB. Figure 1 shows the experimental setup, sensor location and source location over the rail.

PLB experiments were performed at various locations on the rail (as shown in figure 2) to analyse the signal variation and create a dataset for the training and testing of algorithms. PLB experiments were performed at 336 different points, and data from the two sensors were collected. The location of the lead break is marked with reference to the centre between sensor 1 and sensor 2. Details on the locations of experiments are shown in table 1.

### 2.2. Bending experiment for AE signal generation due to crack opening in the rail section

A train moving over a rail track imposes a dynamic load on the rail surface with variable amplitudes. The train movement generates an alternating cycle of tensile and compressive stress, thereby causing damage in the rail section as it suddenly opens and closes. This results in the development of AE waves, which are caused by the formation of a plastic zone at the crack tip and subsequent propagation of the crack subjected to the fatigue cycle. By recording and analysing such signals, one can better understand the degree of damage. A three-point bending experiment on an inverted rail with transverse damage in the rail head was conducted in the laboratory to replicate AE generation due to a crack opening. The test specimen was a 1500 mm long rail piece with 38% head area transverse damage in the centre. Sensors were located in exactly the same location as in the PLB experiment. Figures 3 and 4 show detailed schematics of the inverted rail bending test and actual experiment setup respectively. The specimen was loaded using a compressive loading machine equipped with a bending load arrangement. Three different loadings were applied to the specimen: 100 kN, 150 kN and 200 kN.

3. Proposed schemes for source zone and location classification

The behaviours of the AE waves generated by PLBs at different zones of the rail, namely head, web and foot, are different. Similarly, variations may also be observed with the locations of AE sources with respect to the position of sensors along the length of the rail. Conventional methods involving the relationship between time of flight, wave velocity, wave modes etc., have limitations for AE source localisation in rails. Pattern recognition algorithms such as deep neural networks can notice the change in wave output with respect to the source location. Hence, the location may be predicted by analysing the change in pattern using powerful tools such as deep neural network algorithms. The problem of locating an AE source in a rail can be divided into two parts: the zone of the rail and location along the length. The first algorithm was trained and tested
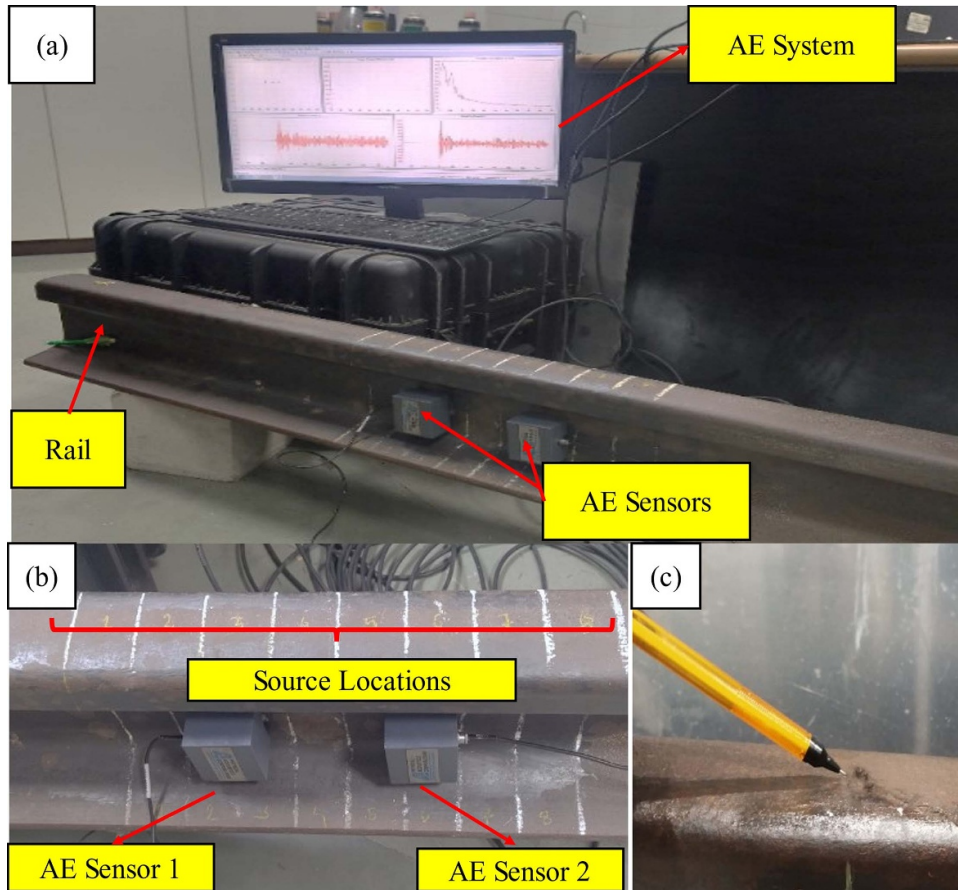
Figure 1. Experimental setup: (a) AE system and sensor, (b) location of lead break source and sensors, (c) pencil lead break (simulated AE source).
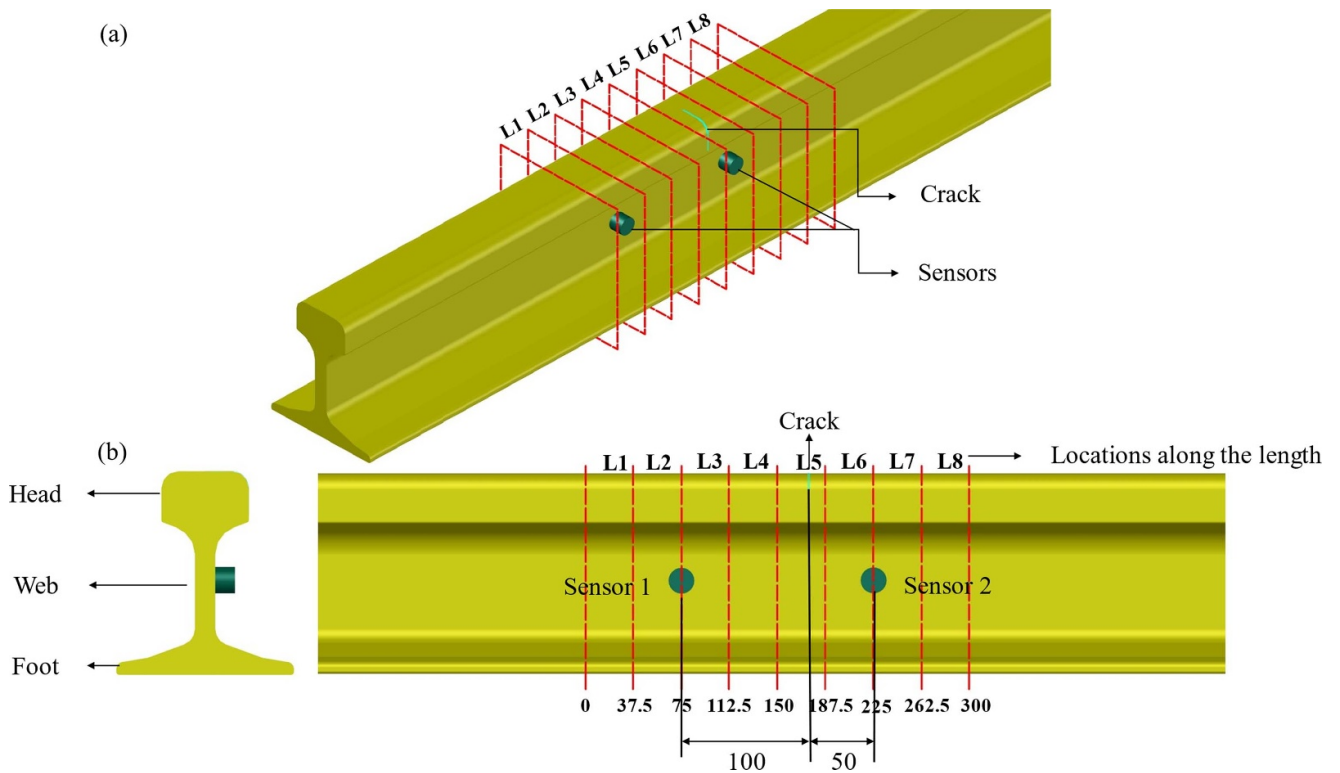
Figure 2. Schematic for locations of PLB experiments over a rail: (a) three-dimensional view (b) section and elevation.

Table 1. Dataset for the lead break source.

		Location								Total
		L1	L2	L3	L4	L5	L6	L7	L8	
Zone	Head	14	14	14	14	14	14	14	14	112
	Web	14	14	14	14	14	14	14	14	112
	Foot	14	14	14	14	14	14	14	14	112
	Total	42	42	42	42	42	42	42	42	336
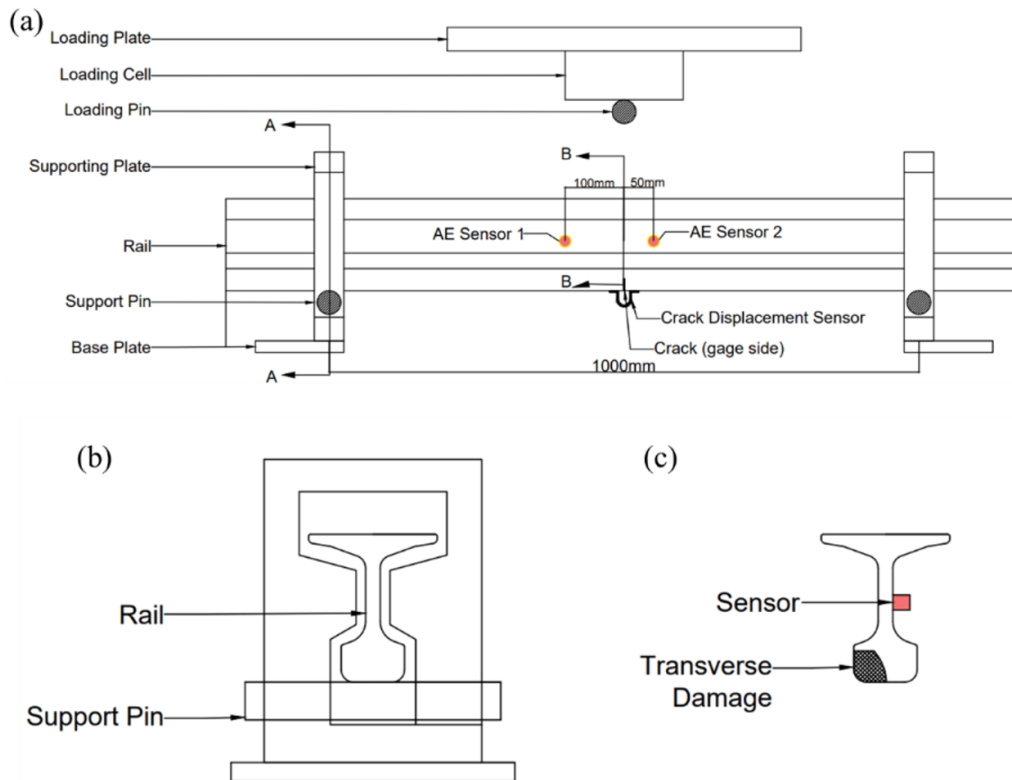
Figure 3. Experimental setup for a three-point bending test on an inverted rail: (a) front view, (b) rail section with support plate, (c) location of AE sensor and crack.

to identify the zone of the rail section where the AE source exists. Next, separate algorithms were trained and tested for each zone to predict the location of the AE source along the length of the rail. Figure 5 shows a flowchart of the proposed scheme. Combining the outcomes of these algorithms can help in locating the AE source within the complex geometry of the rail section. For both algorithms, three neural network structures were worked out, namely ANN, 1DCNN and 2DCNN.

An ANN is a computing algorithm that imitates the neural network of the human brain. An ANN consists of a set of nodes or neurons [30]. Neurons are interconnected, providing a network topology comparable to that of the biological brain network, the source of human intelligence. Each layer of an ANN contains a finite number of neurons. An ANN has input, hidden and output layers. These neurons are the primary prediction-generating processing units of the neural network. In this investigation, a neural network with complete

connectivity is utilised, in which all neurons between layers are interconnected. Figure 6(a) displays the architectural layout of the proposed ANN. Every input is independently weighted, and the sum of weighted inputs is processed by a linear or nonlinear activation function.

SoftMax is utilised in the output layer to solve multiclass problems. The program returns a probability between 0 and 1, which is an indicator of the data sample belonging to a particular class. In all prior layers, tanh, rectified linear activation function (ReLU), Leaky ReLU [31] and scaled exponential linear units (SeLU) [32] are employed. Table 2 shows the different activation functions used in hidden layers. A CNN is a deep learning algorithm having a grid-like data processing algorithm. The input of a 1DCNN is a time series, while that of a 2DCNN can be a red/green/blue (RGB) colour image having three dimensions. The first and second dimensions of a colour image represent the width and height of each image,
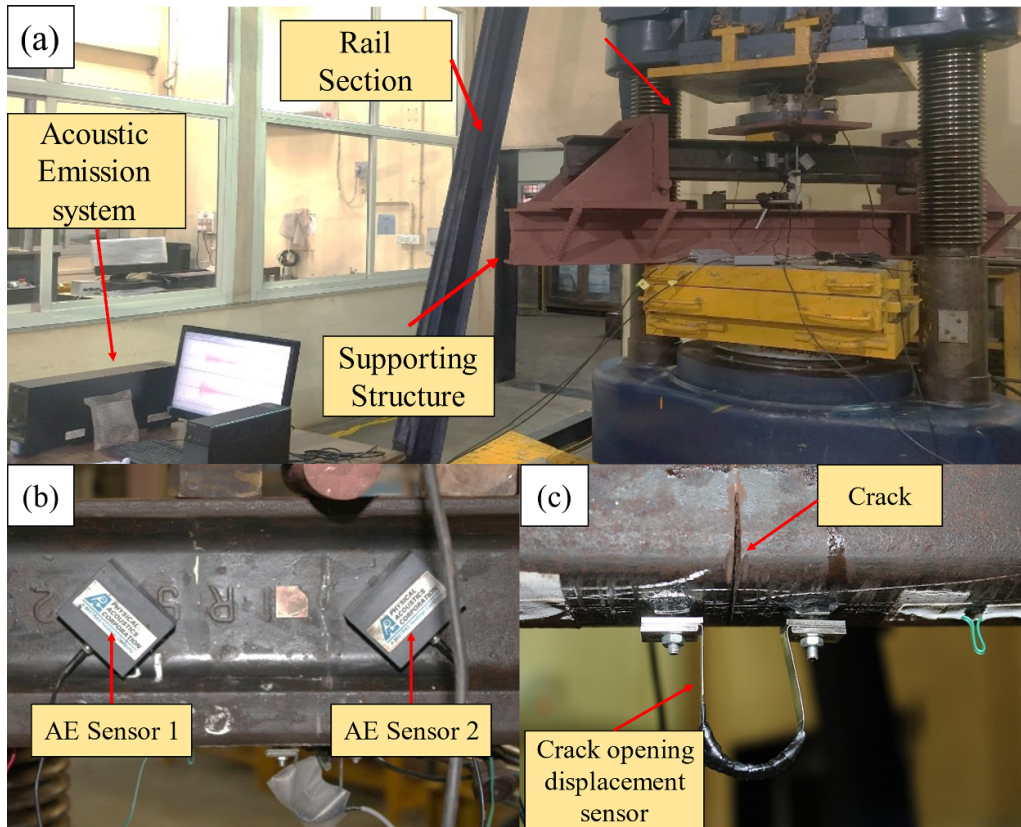
Figure 4. Pictures of the actual experimental setup: (a) three-point bending setup and AE system, (b) AE sensors, (c) crack and crack opening displacement sensor.

respectively. The third dimension corresponds to the RGB colour channels. Change in the location of the AE source causes a relative waveform shift in both sensors. The scalogram generated using the CWT displays wavelet coefficients on a time and frequency scale. A change in position produces a shift in the relative magnitude of the wavelet coefficient, resulting in a change in the RGB concentration of the scalogram image. This change in colour concentration can be correlated with the location of the AE source and is detected by a 2DCNN. Figure 7 shows the input for ANN, 1DCNN and 2DCNN used for the localisation of the AE source in a rail. A CNN has two architectural benefits compared with an ANN. First, information can be weight-shared by introducing a filter or kernel across layers, requiring fewer training parameters than a fully connected feedforward network. Secondly, the local receptive field also enables the CNN to recognise geometric elements such as lines and edges. The parameters 'stride' and 'padding' determine the convolutional layer's receptive fields. In the 2DCNN, the stride parameter determines the amount of vertical and horizontal filter movement, while in the 1DCNN the filter only moves vertically. The spectral feature extraction of the image increases when the stride value is decreased. Padding aids in adding extra rows and columns to the exterior dimensions of an image in order to preserve information from corners and edges. In the proposed method, the stride value was kept at 1 to capture every detail of the input image,

while padding was maintained such that the output has the same dimensions as the input to capture information from the image's corners and edges. The CNN structure is made up of several convolutional and pooling layers that are responsible for analysing AE signals, and dense layers that are responsible for classifying AE sources. Figures 6(b) and (c) exhibit the suggested Conv1D and Conv2D architectures, respectively. After adjusting the activation function and hyperparameters, such as the number of epochs, mini-batch size and learning rate, the most accurate models will be compared and carefully chosen. The top models for zone classification and location classification will be used to test the location of cracks in a rail section.

4. Signal processing and data preparation

4.1. Signal filtering and normalisation

Filtering is needed to isolate useful information from the raw signal by eliminating unwanted components, i.e. noise. Through digital signal processing, digital filters of various types can be utilised for such tasks. An acoustic signal is susceptible to low- and high-frequency noise with varying amplitudes and needs to be filtered before further analysis. In this study, an infinite impulse response (IIR) filter has been considered because, for a given filter order, it exhibits the much
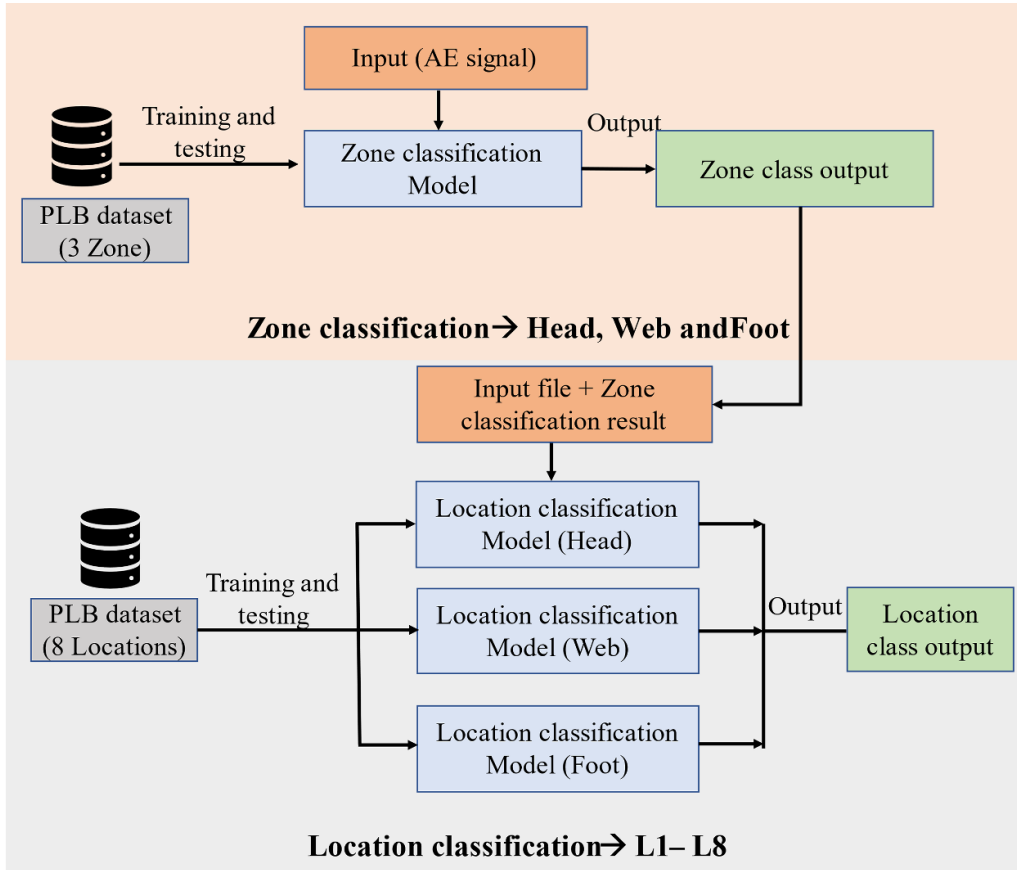
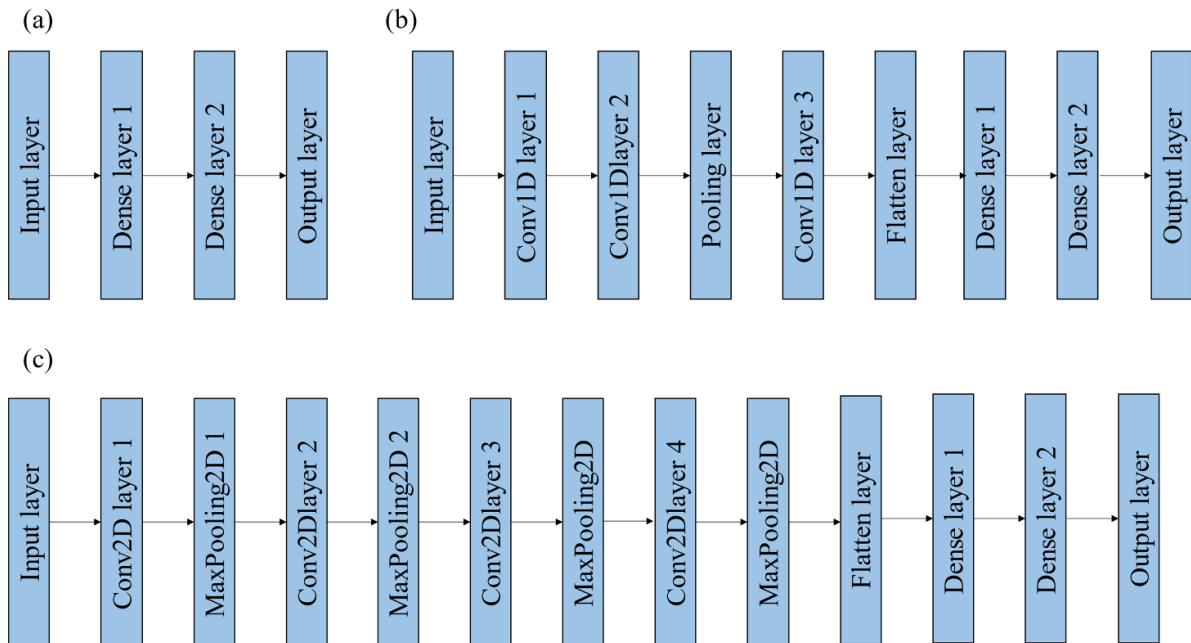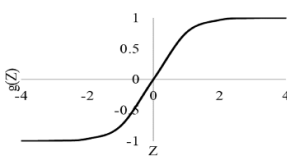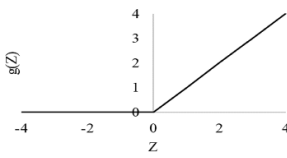**Figure 5.** Flowchart for AE source localisation in a rail section.

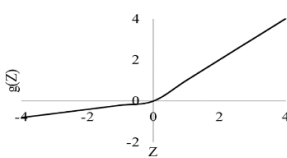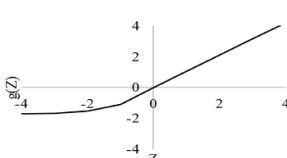**Figure 6.** Architecture of the deep learning models: (a) ANN, (b) 1DCNN and (c) 2DCNN.

sharper transition required for proper filtering of noise from an acquired acoustic signal [33]. In the IIR digital filter an elliptic filter was used as it could achieve a sharper cut-off than a Chebyshev filter. The filter details are provided in table 3. The frequency range was chosen based on the operating frequency range of the sensors.

Table 2. Activation functions.

Sample no.	Activation function	Expression	Plot
1.	Tanh	$g(Z) = \dfrac{e^Z - e^{-Z}}{e^Z + e^{-Z}}$	
2.	Rectified linear unit (ReLU)	$g(Z) = \max\{0, Z\}$	
3.	Leaky ReLU	$g(Z) = \begin{cases} Z \text{ if } Z > 0 \\ \alpha Z \text{ if } Z \le 0 \end{cases}$ Here $\alpha = 0.1$	
4.	Scaled exponential linear unit (SeLU)	$g(Z) = \lambda \begin{cases} Z \\ \alpha(e^Z - 1) \end{cases}$ Here $\alpha = 1.673 \ \lambda = 1.051$	
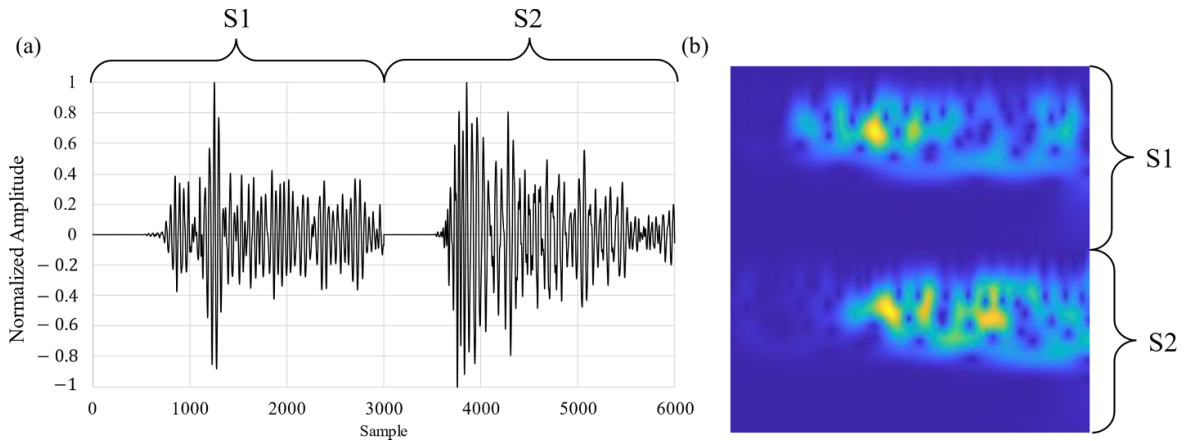
Figure 7. Example of inputs for algorithms (a) for the ANN and 1DCNN and (b) for the 2DCNN.

Table 3. Filter design parameter.

Parameter	Value
Response type	IIR
Design method	Elliptic
Exactly match	Passband
Filter order	4
Sampling frequency	10 000 kHz
First stopband frequency	125 kHz
First passband frequency	150 kHz
Second passband frequency	600 kHz
Second stopband frequency	650 kHz

The fracture of the pencil lead against the surface generates an AE signal in the specimen. However, the energy released from each PLB may be different due to the difference in lengths of the leads, the angle between the lead and the surface while breaking, applied force, etc. Signals received at the sensors may have a different range of values. Hence, normalisation of signals is especially important for correctly interpreting and comparing AE signals. To scale the captured

signal to be within a specific range $[-1, +1]$, a general method is to normalise the wave signal with respect to its maximum and minimum values [34]. Min–max normalization is given by equation (1)

$$F_{\text{new}} = \left(\frac{f_{\text{old}} - \text{Min}_{\text{old}}}{\text{Max}_{\text{old}} - \text{Min}_{\text{old}}} \right) (\text{Max}_{\text{new}} - \text{Min}_{\text{new}}) + \text{Min}_{\text{new}}$$

(1)

where $\text{Max}_{\text{new}} = 1, \text{Min}_{\text{new}} = -1, \text{Min}_{\text{old}} = $ minimum value of the original signal, $\text{Max}_{\text{old}} = $ maximum value of the original signal. Max–min normalisation is a linear transformation that maintains all the information with relationships included in the original signal.

4.2. Wavelet transform

Fourier transform only provides information about the frequency domain. To generate an input image for pattern recognition algorithms, it is required to have time-localised frequency information. Short-time Fourier transform (STFT) and wavelet transform are the methods for generating time–frequency information for a signal. A wavelet transform utilises dilation and transition parameters to represent the signal in the frequency and time domains [35]. CWT of the signal can be carried out using a mother wavelet, resulting in wavelet coefficients for a different times and pseudo-frequencies. The value of the wavelet coefficient and its association with time and frequency is a vital feature of a signal. The CWT coefficients are generated using equation (2)

$$\text{CWT}(a,b) = (f, \psi_{a,b}) = \frac{1}{\sqrt{a}} \int_{-\infty}^{\infty} f(t)\, \psi^* \left(\frac{t-b}{a} \right) \mathrm{d}t.$$

(2)

Compared with STFT, CWT applies an orthogonal filter bank over the entire signal. In this way, one can generate a signal resolution pattern ranging from coarse to fine in the time–frequency domain. This high-resolution RGB image offers critical information regarding the pattern change in the AE signal in relation to the location of the damage. Therefore, this study used CWT to produce inputs for the 2DCNN.

4.3. Data preparation

A total of 336 PLB experiments were carried out. These data were utilised for training and testing AI-based algorithms for zone and location classification. All the signals were corrupted to incorporate the effect of noise by adding white Gaussian noise of amplitude 5%, 10%, 15% and 20% of the main signal amplitude. This makes the dataset comprise a total 1680 signals generated from three parts, namely head, web and foot, and at various locations L1–L8. The dataset containing the original signals was divided into training and testing data in the

ratio 70:30 before adding noise to avoid the problem of data leakage, which may occur due to a randomised train–test split.

Each sensor had an AE signal of the length of 3000 samples based on sampling rate $(1 \times 10^7$ samples s$^{-1})$ and time of signal recording (300 μs). The input was provided differently for different algorithms. For the ANN and 1DCNN, only the time series data were required. For the 2DCNN, continuous wavelet transformation of a one-dimensional signal was carried out to generate the time–frequency representation of a signal, which is called a scalogram. The scalogram is then stored as an image file with three layers of information in RGB colour concentrations. Figure 7 shows the inputs for the ANN, 1DCNN and 2DCNN.

5. Results and discussion

5.1. Results for PLB at various zones of the rail section

The output from the PLB at the head, web and foot in location zone 4 is shown in figure 8. It can be observed that even for the same PLB source location, the waveforms generated at the different zones, i.e. head, web and foot, are different. In the case of the head, the dispersion of the wave over time can be noticed, while in the case of the web, the waveform has a specific peak with less dispersion. Since the sensors are attached to the web, the clear peak of the wave can first be observed on the web. The foot is thinner than the head; hence, less dispersion is observed. Due to the dispersive characteristics of waves in the rail and the generation of the waveform over a broad frequency, it is difficult to identify the zone of the AE source. However, by analysing the pattern of some distinct parameters, such as dispersion, time of arrival and energy concentration, it is possible to identify the zone of the AE source. The deep learning algorithm can help in observing such a pattern change.

5.2. Result of deep learning algorithms on the testing dataset of the AE signal in a rail

The output received from the AE system for a PLB is corrupted with white noise of varying amplitude, creating a noisy dataset to replicate the effect of field testing. All these signals are then filtered and normalised. Later, the dataset is converted into the array and scalogram images as inputs for various algorithms. A total of 1680 signals are provided as input, among which 1200 were used for training and 480 for testing. After completion of the training, all the models are validated using the testing dataset. Overall accuracy can be used to compare the efficiency of any given algorithm. Figure 9 shows a comparison of the accuracy of various models for zone classification. Among all the algorithms, 2DCNN with the SeLU activation function performed best for zone classification with an accuracy of 94.79% on the testing data. All algorithms are again trained and tested for location classification along the length of rail. Here, the output layer is modified for eight location zones. The algorithm attempts to observe pattern change in the signal of both sensors with respect to location. Figure 10 shows the accuracy of various algorithms with the testing data
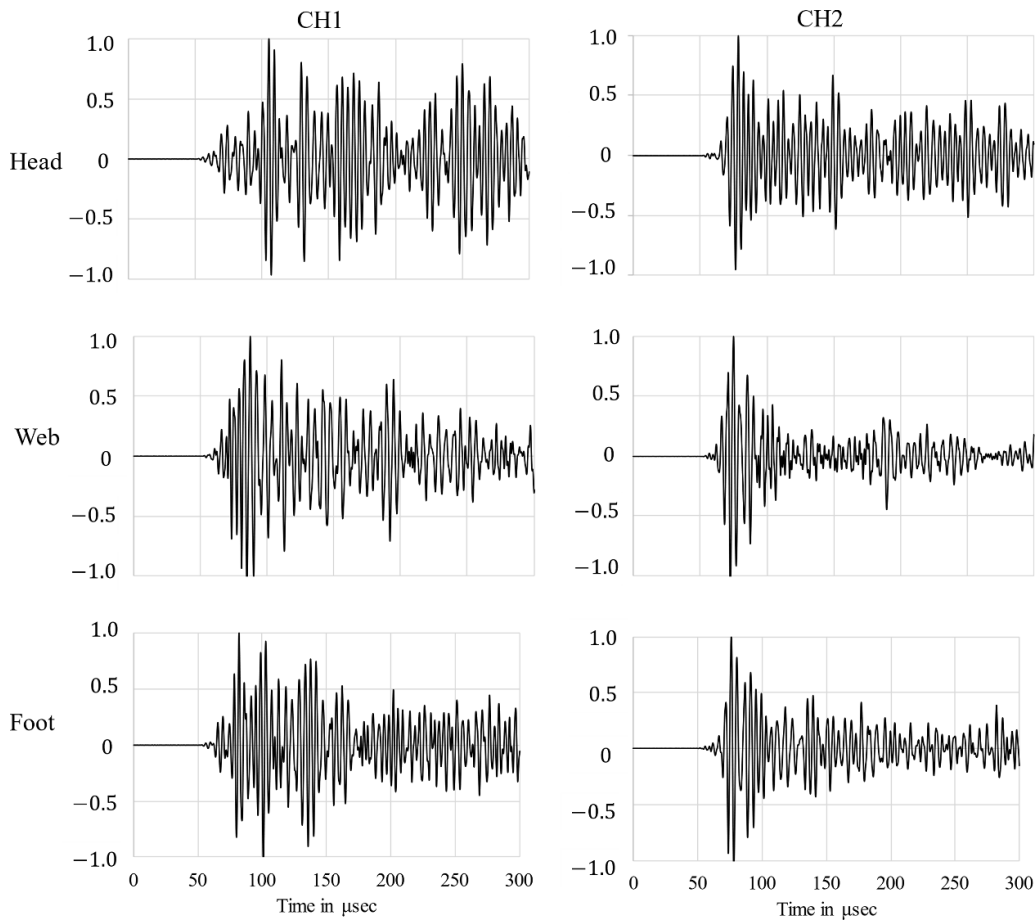
Figure 8. Time history of the acoustic signal generated due to PLB at various zones of the rail in location L4 (*x*-axis: time in µs, *y*-axis: normalised amplitude).
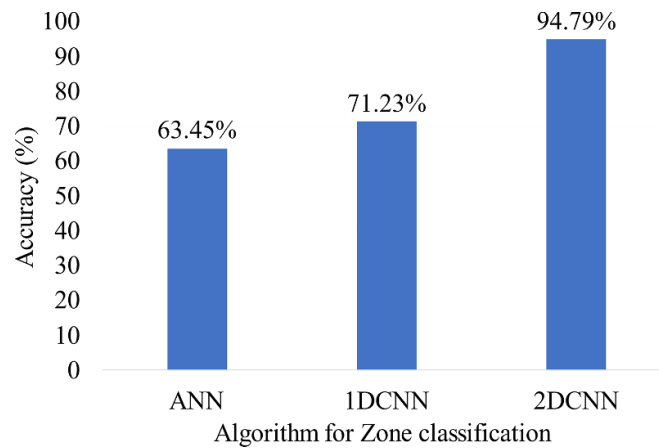
Figure 9. Testing accuracy for zone identification of an AE source in the rail.

of location classification. Even for location classification along the length, 2DCNN with the SeLU activation function outperformed other algorithms in all three zones. ANN/CNN lead by a gradient-based process known as backpropagation. In the ReLU activation function the problem of a vanishing gradient arises where learning can stop. SeLU cannot have a vanishing gradient and hence it has better performance than ReLU. In a classification task, the confusion matrix indicates the relative

accuracies for each class. The confusion matrix for the best performing algorithm for zone and location classifications is shown in figure 11. Table 4 presents performance metrics for zone classification test results, such as recall, precision and F1 score. Table 5 also provides the performance metrics for location classification along the length for each of the three zones, head, web and foot. The AE signals are easily distinguishable for the three rail zones, resulting in very good accuracy. The
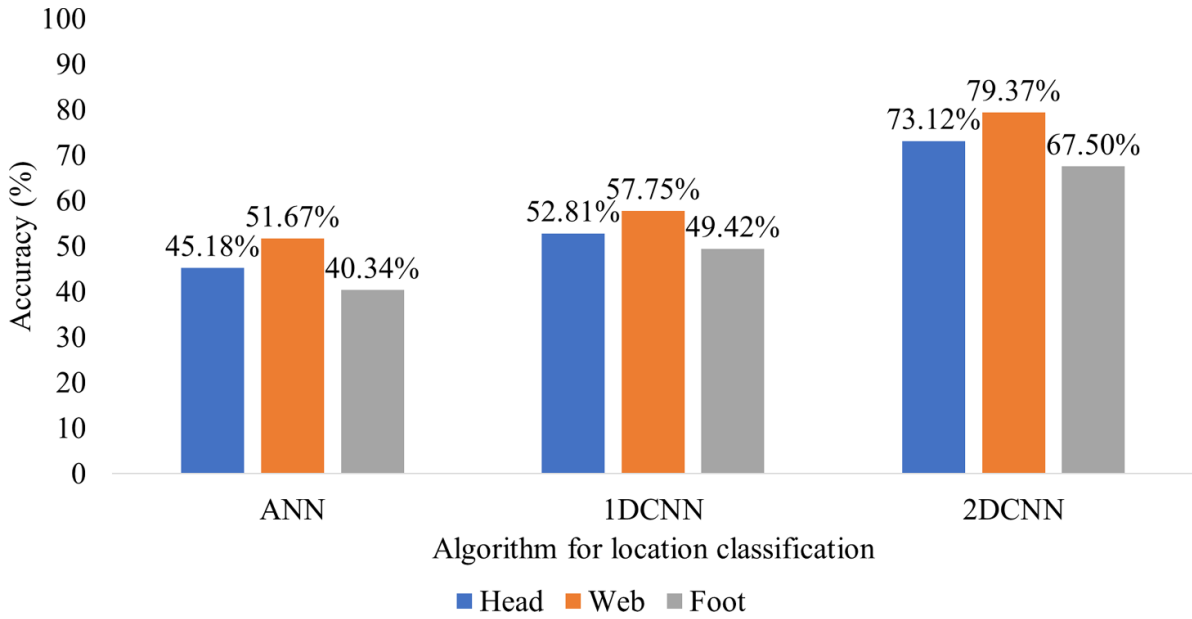
Figure 10. Testing accuracy for location zone identification of an AE source in the rail.
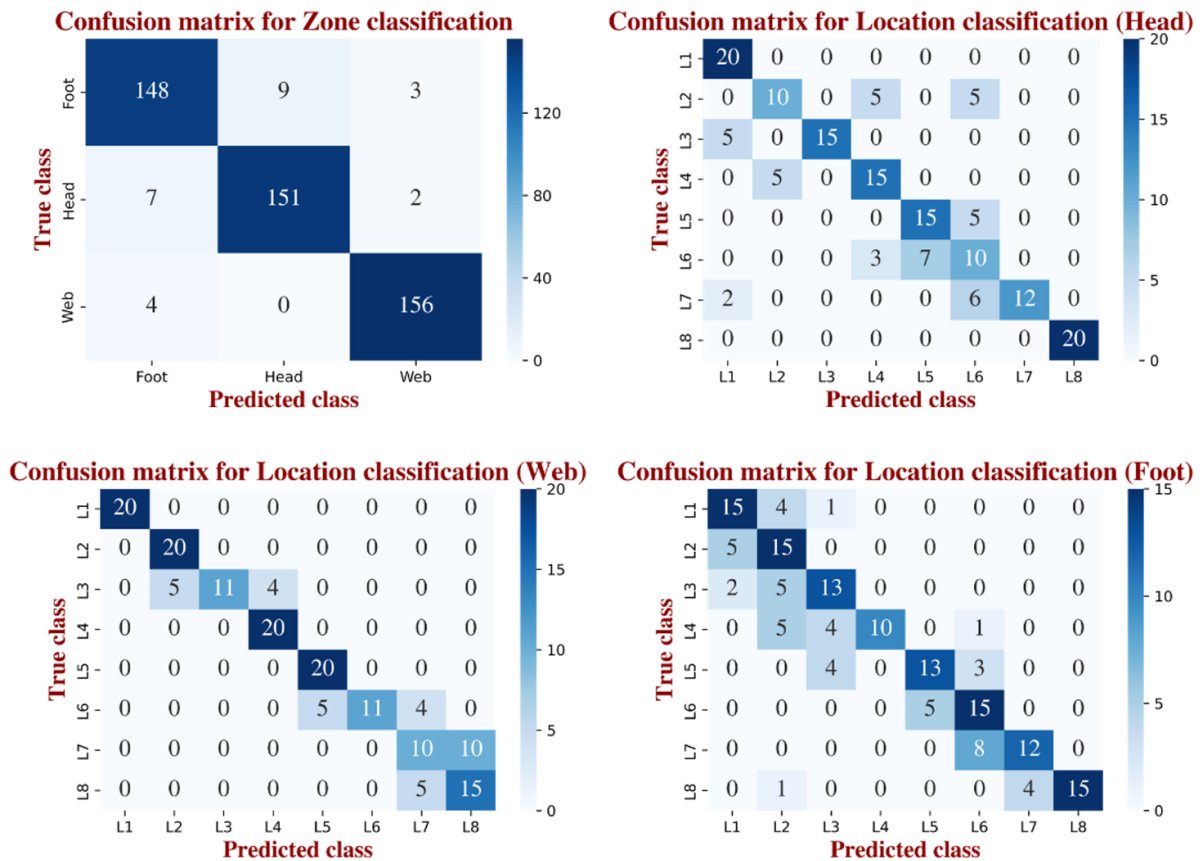
Figure 11. Confusion matrix of testing data for the best algorithms for zone classification and location along the length.

accuracies for location classification along the length for head, web and foot are lower because there are only slight changes in signal for adjacent locations along the length. In the head and foot, the signals reaching the sensor, which is located at the web, had a lot of dispersion and hence their accuracies are low. In the web, the signal suffers less dispersion, resulting in good accuracy. In all three zones, the accuracies are much better than random guessing.

Table 4. Performance metrics for zone classification of an AE source in a rail.

| Zone	R (%)	P (%)	F1
Foot	93.08	94.37	96.89
Head	92.50	94.37	97.50
Web	92.78	94.37	97.19

Table 5. Performance metrics for location classification of an AE source in a rail along the length.

Location	Head			Web			Foot		
	R (%)	P (%)	F1	R (%)	P (%)	F1	R (%)	P (%)	F1
L1	100	74.07	85.11	100	100	100	75	68.18	71.42
L2	50	66.67	57.14	100	80	88.88	75	51.72	61.22
L3	75	100	85.71	55	100	70.96	65	59.09	61.9
L4	75	65.21	69.76	100	83.33	90.91	50	100	66.67
L5	75	68.18	71.42	100	80	88.88	65	72.22	68.42
L6	50	38.46	43.47	55	100	70.96	75	55.55	63.82
L7	60	100	75	50	52.63	51.28	60	70.58	64.86
L8	100	100	100	75	60	66.67	75	100	85.71

R, recall; P, precision; F1, F1 score.
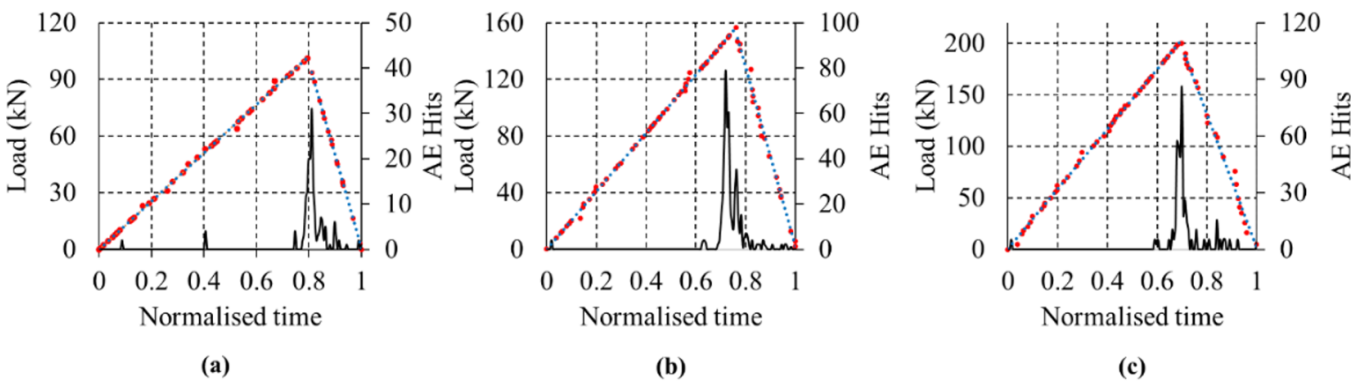
Figure 12. Time versus load and AE hit: (a) 100 kN, (b) 150 kN and (c) 200 kN.

5.3. Result of algorithms on output from the bending experiment

Deep learning algorithms were trained and tested for the classification of zone and location of an AE source along the length by using a dataset generated from a simulated AE source, i.e. a PLB. Based on accuracy and other performance metrics, 2DCNN with the SeLU activation function outperformed other algorithms. Combining the outputs of zone and location classification algorithms results in location of the AE source in the rail. To deploy the trained algorithm, the .h5 file of the model is extracted and saved. The '.h5' file format [36] stores the structured data of weights and the configuration of a trained model, which can be deployed and used to predict results for new inputs. The model is then used to generate outputs for new AE signals. To simulate AE signal generation from a crack opening in rail, a bending test on an inverted damaged rail was conducted with loads of 100 kN, 150 kN and 200 kN. Figure 12 shows the application of the load and the increase in AE hits with respect to it. The AE signal observed at peak load is considered for analysis. AE signals obtained from the bending experiment are filtered and normalised. Scalogram images are generated using CWT, as discussed in section 4.2. Generated images are then used as input for trained algorithm to determine the location of the AE source. The inputs are provided to both algorithms to identify both zone and location along the length in the rail section. The outputs from the SoftMax layer of the 2DCNN result in the probability of each class. Figure 13 shows the probability of the AE source being located in each zone of the rail section. It can be observed that a high probability is found for the AE source lying in the head. Algorithms show the accurate prediction for the zone class for each load. Except for the 100 kN load, location class was predicted accurately. This approach proves to be promising due to the similarity between the AE signal generated from the PLB source and crack opening.
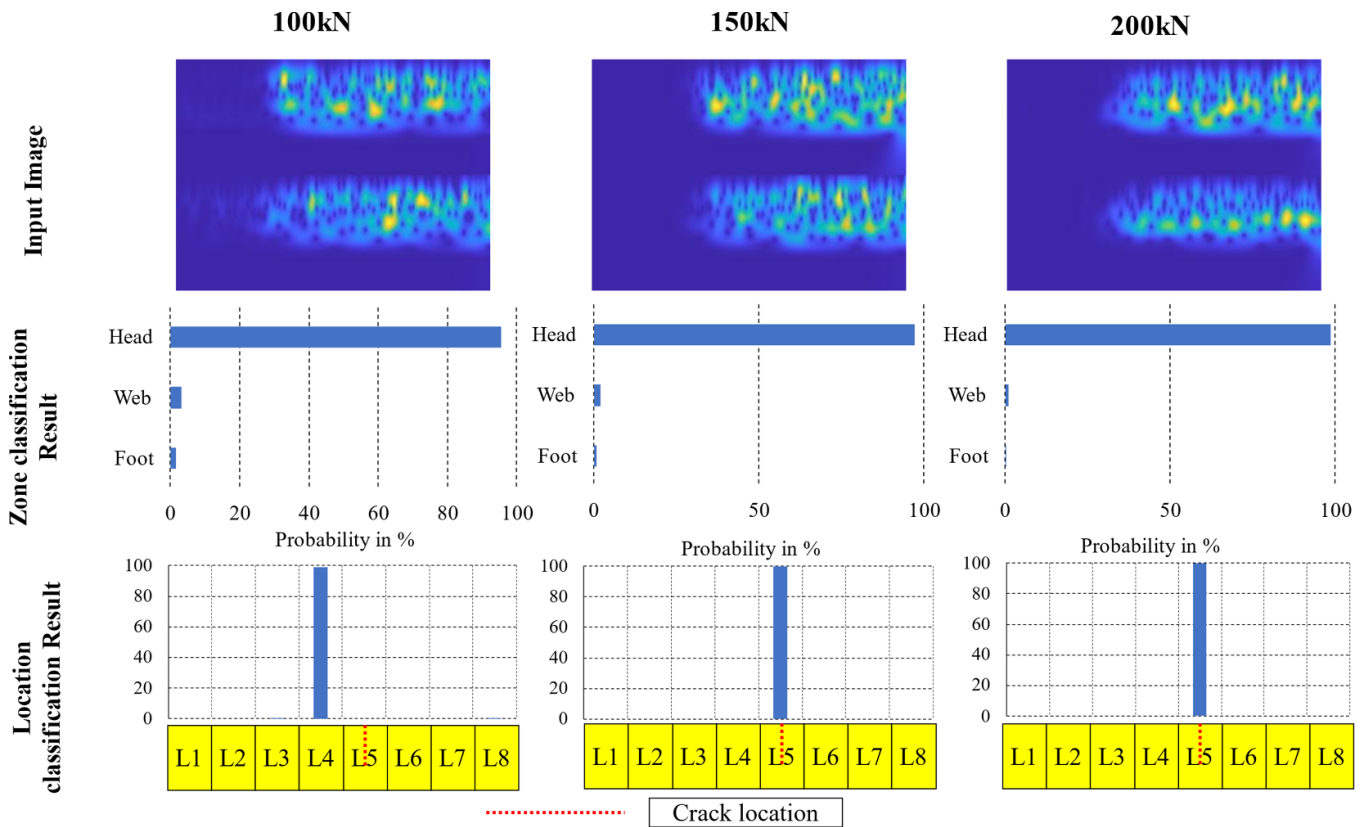
Figure 13. Output result for an AE source in the rail head, web and foot.

6. Conclusion

Due to the presence of multiple modes, excessive noise and the broad frequency spectrum of AE signals, AE testing of rails is a challenging task. Prior to completing any analysis on rail damage, it is necessary to locate the AE source. However, for a complex section such as a rail, conventional analysis methods based on velocity and time of flight are complicated and ineffective. This study proposes acoustic source localisation in the rail section by utilising AE waveform parameters. A PLB source was initially used as a simulated AE source to generate training and testing data. Deep learning algorithms were trained and tested based on the dataset to locate the AE source. Then trained algorithms were deployed to determine the location of the AE signal generated by the crack opening in the rail under a bending load. The localisation of the AE source in rail was divided into two parts: zone of the rail and location along the length of the rail. For both problems, three algorithms were used: ANN, 1DCNN and 2DCNN.

The following conclusions can be drawn from this study:

The experiments indicate distinctive patterns of AE waveforms generated in different rail zones.

(a) 2DCNN with the proposed architecture demonstrated the highest accuracy of 94.79% on testing data for the identification of the rail zone in which the AE source is located.
(b) Similarly, for the identification of the location of the AE source along the length of the rail, 2DCNN with the proposed architecture shows good accuracy of 73.12%,

79.37% and 67.50% for locating an AE source in the head, web and foot, respectively.
(c) A deep learning algorithm effectively reduces the manual effort of feature extraction. This methodology captures every pattern change and assigns it to various classes.
(d) The models prepared were applied over the AE signal generated from crack opening in an actual rail section. For all three applied loads, the highest probability of location was observed in the head zone. For crack opening under 150 kN and 200 kN loads, the location of the AE signal generated from a crack in the rail was predicted accurately.

Due to attenuation in rail sections and limitations of the present sensors and data acquisition system, the AE test in this study was limited to a small section of rail only. However, the proposed methodology assists in determining the location of an AE source in a rail and can be used for further investigation, such as determining the severity of damage in a field test. Additionally, this study stands as a proof of concept for the employment of AI-based algorithms to evaluate damage parameters such as type, source location and severity in real time via AE in extremely complicated geometries such as rails.

Data availability statement

The data that support the findings of this study are available upon reasonable request from the authors.

Acknowledgments

The authors want to acknowledge Jindal Steel & Power Limited for providing rail sections for the experiments

ORCID iD

Harsh Mahajan https://orcid.org/0000-0002-9295-8261

References

[1] Bruzelius K and Mba D 2004 An initial investigation on the potential applicability of acoustic emission to rail track fault detection *NDT&E Int.* **37** 507–16

[2] Bollas K, Papasalouros D, Kourousis D and Anastasopoulos A 2010 Acoustic emission inspection of rail wheels *J. Acoust. Emiss.* **28** 215

[3] Zhang X, Feng N, Wang Y and Shen Y 2014 An analysis of the simulated acoustic emission sources with different propagation distances, types and depths for rail defect detection *Appl. Acoust.* **86** 80–88

[4] Hao Q, Wang Y, Yi S and Zhang X 2015 De-noising of rail crack AE signal based on wavelet modulus maxima *Conf. Record—IEEE Instrumentation and Measurement Technology Conf.* (July 2015) pp 675–80

[5] Bianchi D, Mayrhofer E, Gröschl M, Betz G and Vernes A 2015 Wavelet packet transform for detection of single events in acoustic emission signals *Mech. Syst. Signal Process.* **64–65** 441–51

[6] Kuang K S C, Li D and Koh C G 2016 Acoustic emission source location and noise cancellation for crack detection in rail head *Smart Struct. Syst.* **18** 1063–85

[7] Li D, Kuang K S C and Koh C G 2017 Fatigue crack sizing in rail steel using crack closure-induced acoustic emission waves *Meas. Sci. Technol.* **28** 65601

[8] Zhang X, Zou Z, Wang K, Hao Q, Wang Y, Shen Y and Hu H 2018 A new rail crack detection method using LSTM network for actual application based on AE technology *Appl. Acoust.* **142** 78–86

[9] Zhang X, Sun T, Wang Y, Wang K and Shen Y 2020 A parameter optimized variational mode decomposition method for rail crack detection based on acoustic emission technique *Nondestruct. Test. Eval.* **36** 1–29

[10] Ohtsu M and Ono K 1988 AE source location and orientation determination of tensile cracks from surface observation *NDT Int.* **21** 143–50

[11] Ciampa F and Meo M 2010 A new algorithm for acoustic emission localization and flexural group velocity determination in anisotropic structures *Composites* A **41** 1777–86

[12] Dehghan Niri E and Salamone S 2012 A probabilistic framework for acoustic emission source localization in plate-like structures *Smart Mater. Struct.* **21** 035009

[13] Mostafapour A, Davoodi S and Ghareaghaji M 2014 Acoustic emission source location in plates using wavelet analysis and cross time frequency spectrum *Ultrasonics* **54** 2055–62

[14] Al-Jumaili S K, Pearson M R, Holford K M, Eaton M J and Pullin R 2016 Acoustic emission source location in complex structures using full automatic delta T mapping technique *Mech. Syst. Signal Process.* **72–73** 513–24

[15] Mirgal P, Pal J and Banerjee S 2020 Online acoustic emission source localization in concrete structures using iterative and evolutionary algorithms *Ultrasonics* **108** 106211

[16] Agarwal S and Mitra M 2014 Lamb wave based automatic damage detection using matching pursuit and machine learning *Smart Mater. Struct.* **23** 085012

[17] Das A K, Suthar D and Leung C K Y 2019 Machine learning based crack mode classification from unlabeled acoustic emission waveform features *Cem. Concr. Res.* **121** 42–57

[18] Tsai T-C and Wang C-N 2022 Acoustic-based method for identifying surface damage to wind turbine blades by using a convolutional neural network *Meas. Sci. Technol.* **33** 85601

[19] Ai L, Soltangharaei V, Bayat M, Tooren M and Ziehl P 2021 Detection of impact on aircraft composite structure using machine learning techniques *Meas. Sci. Technol.* **32** 84013

[20] Liu W, Tang Z, Lv F and Chen X 2022 An efficient approach for guided wave structural monitoring of switch rails via deep convolutional neural network-based transfer learning *Meas. Sci. Technol.* **34** 24004

[21] Muir C, Swaminathan B, Fields K, Almansour A S, Sevener K, Smith C, Presby M, Kiser J D, Pollock T M and Daly S 2021 A machine learning framework for damage mechanism identification from acoustic emissions in unidirectional SiC/SiC composites *NPJ Comput. Mater.* **7** 146

[22] Suwansin W and Phasukkit P 2021 Deep learning-based acoustic emission scheme for nondestructive localization of cracks in train rails under a load *Sensors* **21** 272

[23] Ebrahimkhanlou A, Dubuc B and Salamone S 2019 A generalizable deep learning framework for localizing and characterizing acoustic emission sources in riveted metallic panels *Mech. Syst. Signal Process.* **130** 248–72

[24] Hesser D F, Mostafavi S, Kocur G K and Markert B 2021 Identification of acoustic emission sources for structural health monitoring applications based on convolutional neural networks and deep transfer learning *Neurocomputing* **453** 1–12

[25] Sikdar S, Liu D and Kundu A 2022 Acoustic emission data based deep learning approach for classification and detection of damage-sources in a composite panel *Composites* B **228** 109450

[26] Barbosh M, Dunphy K and Sadhu A 2022 Acoustic emission-based damage localization using wavelet-assisted deep learning *J. Infrastruct. Preserv. Resilience* **3** 1–24

[27] Li D, Wang Y and Yan W-J 2020 Acoustic emission wave classification for rail crack monitoring based on synchrosqueezed wavelet transform and multi-branch convolutional neural network *Struct. Health Monit.* **20** 1563–82

[28] Mahajan H and Banerjee S 2021 A machine learning framework for guided wave-based damage detection of rail head using surface-bonded piezo-electric wafer transducers *Mach. Learn. Appl.* **7** 100216

[29] Zelenyak A M, Hamstad M A and Sause M G R 2015 Modeling of acoustic emission signal propagation in waveguides *Sensors* **15** 11805–22

[30] Gana M, Achour H, Belaid K, Chelli Z, Laghrouche M and Chaouchi A 2022 Non-invasive intelligent monitoring system for fault detection in induction motor based on

lead-free-piezoelectric sensor using ANN *Meas. Sci. Technol.* **33** 65105

[31] Maas A L, Hannun A Y and Ng A Y 2013 Rectifier nonlinearities improve neural network acoustic models *Proc. 30th Int. Conf. on Machine Learning* (*Atlanta, GA, USA*)

[32] Klambauer G, Unterthiner T, Mayr A and Hochreiter S 2017 Self-normalizing neural networks *Proc. 31st Int. Conf. on Neural Information Processing Systems NIPS'17* (*Long Beach, CA, USA*) pp 972–81

[33] Ingle V K and Proakis J G 2008 *Digital Signal Processing Using MATLAB®* 3rd edn, vol 5 (Stamford, CT: Wiley)

[34] Su Z and Ye L 2009 *Identification of Damage Using Lamb Waves* (London: Springer) (https://doi.org/10.1007/978-1-84882-784-4)

[35] Maria J 2017 *Digital Signal Processing with Matlab Examples* vol 3, ed G Sierra (Singapore: Springer) (https://doi.org/10.1007/978-981-10-2534-1)

[36] Wu K and Chollet F 2020 *Serialization and saving* (available at: https://tensorflow.rstudio.com/guides/keras/serialization_and_saving)